ADVANCED FUNCTIONAL MATERIALS
www.afm-journal.de

Electrically and Magnetically Tunable Valley Polarization in Monolayer $MoSe_2$ Proximitized by a 2D Ferromagnetic Semiconductor

Tongyao Zhang, Siwen Zhao, Anran Wang, Zhiren Xiong, Yingjia Liu, Ming Xi, Songlin Li, Hechang Lei,* Zheng Vitto Han,* and Fengqiu Wang**

The emergence of atomically thin valleytronic semiconductors and 2D ferromagnetic materials is opening up new technological avenues for future information storage and processing. A key fundamental challenge is to identify physical knobs that may effectively manipulate the spin-valley polarization, preferably in the device context. Here, a novel spin functional device that exhibits both electrical and magnetic tunability is fabricated, by contacting a monolayer $MoSe_2$ with a 2D ferromagnetic semiconductor $Cr_2Ge_2Te_6$. Remarkably, the valley-polarization of $MoSe_2$ is found to be controlled by a back-gate voltage with an appreciably enlarged valley splitting rate. At fixed gate voltages, the valley-polarization exhibits magnetic-field and temperature dependence that corroborates well with the intrinsic magnetic properties of $Cr_2Ge_2Te_6$, pointing to the impact of magnetic exchange interactions. Due to the interfacial arrangement, the charge-carrying trion photoemission predominates in the devices, which may be exploited to enable drift-based spin-optoelectronic devices. These results provide new insights into valley-polarization manipulation in transition metal dichalcogenides by means of ferromagnetic semiconductor proximitizing and represent an important step forward in devising field-controlled 2D magneto-optoelectronic devices.

1. Introduction

Monolayer transition metal dichalcogenides (TMDs) have attracted great attentions due to their extraordinary optical and optoelectronic properties.[1–4] The optical selection rules and spin-valley locking effect in TMDs support the optical generation, propagation/modulation, and detection of spin-valley polarization.[5–9] The incorporation of magnetism with TMD-based valley-optoelectronic functionalities, through creation of magnetic semiconductor heterostructures, represents a promising avenue for conceptually novel spintronic devices.[10–15] Proximity-induced exchange interactions have proved effective to control the valley properties of monolayer TMDs in ferromagnetic heterostructure comprising ferromagnetic insulators, such as CrI_3 and $CrBr_3$.[16–18] For example, in the vdW heterostructures of ferromagnetic insulators CrI_3 and monolayer WSe_2, the spin-dependent ultrafast charge hopping, arising from the relative alignment between photocarrier spins in WSe_2 and magnetization of CrI_3, remarkably affects the valley splitting and polarization of WSe_2.[17] Despite the breakthroughs, challenges still remain for fabricating real devices. For example, although a back-gate voltage can precisely control carrier concentrations and polarity, the negligible electrical conductivity in CrI_3 and $CrBr_3$ at low temperatures

T. Zhang, A. Wang, S. Li, F. Wang
School of Electronic Science and Engineering
Nanjing University
Nanjing 210093, China
E-mail: fwang@nju.edu.cn

T. Zhang, Z. Xiong, Z. V. Han
State Key Laboratory of Quantum Optics and Quantum Optics Devices
Institute of Opto-Electronics
Shanxi University
Taiyuan 030006, China
E-mail: zhenghan@sxu.edu.cn

T. Zhang, Z. Xiong, Z. V. Han
Collaborative Innovation Center of Extreme Optics
Shanxi University
Taiyuan 030006, China

S. Zhao, Y. Liu
Shenyang National Laboratory for Materials Science
Institute of Metal Research
Chinese Academy of Sciences
Shenyang 110016, China
E-mail: swzhao@imr.ac.cn

S. Zhao, Y. Liu
School of Material Science and Engineering
University of Science and Technology of China
Anhui 230026, China

M. Xi, H. Lei
Department of Physics and Beijing Key Laboratory of Opto-electronic Functional Materials & Micro-nano Devices
Renmin University of China
Beijing 100872, China
E-mail: hlei@ruc.edu.cn

The ORCID identification number(s) for the author(s) of this article can be found under https://doi.org/10.1002/adfm.202204779.

DOI: 10.1002/adfm.202204779

poses significant challenges for exploring electric field controlled nanodevices.[19,20] In contrast, 2D ferromagnetic semiconductor $Cr_2Ge_2Te_6$ has recently been demonstrated to remain conducting and gate tunable below its ferromagnetic Curie temperature (≈50 K), yielding bipolar field effect transistors with long-range spin ordering.[21–23] The coupling of monolayer TMDs and few-layer $Cr_2Ge_2Te_6$ can thus be of interest for engineering spin-dependent charge transfer with an extra degree of freedom of injected carriers into the junction, and it is also highly desirable to explore the gate-tunable valley physics of excitons in this unprecedented semiconductor heterojunction formed by $Cr_2Ge_2Te_6$ and monolayer TMDs.

Here, we fabricate van der Waals ferromagnetic heterojunctions formed by few-layer $Cr_2Ge_2Te_6$ and monolayer molybdenum diselenide ($MoSe_2$) and study the devices' photoluminescence circular dichroism under different electrical back-gate voltages and temperatures. Remarkably, we found the degree of valley polarization in the heterojunction exhibits clear modulation by external magnetic fields, when biased at a positive gate voltage (≈80 V). This indicates effective spin-dependent charge transfer across the heterointerface, and is in agreement with the increased spectral weight of trion photoemission in the heterojunction region. Further, the effect is seen to disappear when operating above the magnetic Curie temperature (T_C) of $Cr_2Ge_2Te_6$, suggesting impact from the exchange interactions due to the magnetic constituent. Band alignment between $Cr_2Ge_2Te_6$ and $MoSe_2$ is experimentally confirmed by Kelvin probe force microscopy (KPFM), the type-II structure facilitates electron injection from $Cr_2Ge_2Te_6$ to $MoSe_2$ at high positive gate voltages. The valley splitting of trions in the heterojunction was found to be several times larger than that can be achieved by the Zeeman effect in bare $MoSe_2$, evidencing the peculiar interfacial magnetic exchange field. Our findings shed lights on the subtle magnetic proximity effects on the valley properties in heterojunctions made of 2D ferromagnetic semiconductors and TMDs, and pave the way for future valleytronics in opto-electronic applications.

2. Results and Discussion

$Cr_2Ge_2Te_6$ is a layered ferromagnetic semiconductor with an optical gap near 0.4 eV.[23,24] Bulk $Cr_2Ge_2Te_6$ crystal exhibits a T_C of ≈64 K, a saturation magnetization of ≈3 Bohr magneton per Cr, and an out-of-plane easy axis.[25] The typical X-ray diffraction (XRD) pattern of the as-grown $Cr_2Ge_2Te_6$ crystal is shown in Figure S1 (Supporting Information). In order to prevent the degradation of $Cr_2Ge_2Te_6$, we have vertically assembled ≈5–10 nm thick multilayered $Cr_2Ge_2Te_6$ and monolayer $MoSe_2$ (**Figure 1**a) using a state-of-the-art h-BN encapsulation technique in a nitrogen-filled glove box, as shown in Figure 1b (see also Experimental Section).[26,27] The two few-layer graphite flakes act as an electrodes for reducing the contact resistance of $Cr_2Ge_2Te_6$ at low temperatures. Monolayer $MoSe_2$ is side-contacted by Cr/Au via standard lithography and plasma etching.

After the device fabrication, we noticed negligible degradation of $Cr_2Ge_2Te_6$ and this is confirmed by Raman spectroscopy (Figure S2, Supporting Information). There are three characteristic regions of the device, namely zone I (monolayer $MoSe_2$), zone II (few-layer $Cr_2Ge_2Te_6$), and zone III ($Cr_2Ge_2Te_6/MoSe_2$ heterojunction). As shown in Figure 1c, we have measured the field-effect curves of few-layer $Cr_2Ge_2Te_6$ at different temperatures. Note that the transfer characteristics show bipolar transport behaviors at 10–300 K, allowing us to investigate the

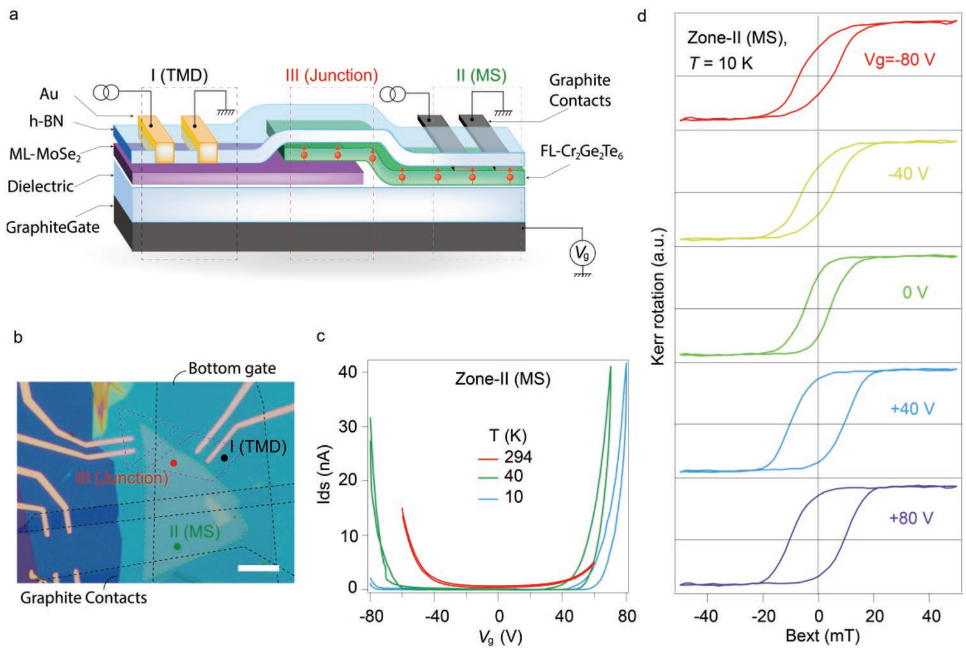

Figure 1. $Cr_2Ge_2Te_6/MoSe_2$ van der Waals heterojunction. a) Schematic diagram of the device showing three different regions. Specifically, region I: bare $MoSe_2$ (TMD), region II: magnetic semiconductor (MS) and region III: the heterojunction. b) Optical microscope image of one typical device. The $Cr_2Ge_2Te_6/MoSe_2$ heterojunction is sandwiched by h-BN. The scale bar is 5 µm. c) Field-effect curves of MS with different temperatures. d) Kerr angle of MS at different gates measured at 10 K.

valley polarization of the heterostructures with both electron and hole doping in $Cr_2Ge_2Te_6$. Note that it takes increasingly large back voltages to induce channel carriers as the temperature is decreased to ≈10 K, and the asymmetric transfer curve indicates that electron-doping is somehow easier in $Cr_2Ge_2Te_6$ at low temperatures. Figure S3 (Supporting Information) plots the transfer characteristics of monolayer $MoSe_2$, indicating that $MoSe_2$ possesses n-type behavior. The rectifying behavior of the *I*–*V* characteristics of the heterojunction clearly demonstrates the built-in potential at the interface of $MoSe_2$ and $Cr_2Ge_2Te_6$. In addition, we have also studied the gate dependent magneto-optic Kerr effect in $Cr_2Ge_2Te_6$. When the temperature is below the T_C of $Cr_2Ge_2Te_6$, magnetic hysteresis loops of $Cr_2Ge_2Te_6$ appear and can be significantly tuned by the gate voltage. Upon carrier doping, both saturation field (H_S) and coercivity (H_c) exhibit bipolar characteristics, as shown in Figure 1d.

2.1. Polarization-Resolved Magneto-Photoluminescence in Monolayer $MoSe_2$ and $Cr_2Ge_2Te_6$/$MoSe_2$ Heterostructure

We then investigate the photoluminescence characteristics of the fabricated devices. **Figure 2**a shows the schematic crystal structure of the heterojunction. We focus on measurement at 10 K, which is well within the T_C of the magnetic constituent. PL spectra for different regions of the devices at 10 K are shown in Figure 2b,c, using 10 μW laser excitation centered at 1.75 eV. For both monolayer $MoSe_2$ and the heterojunction, trion emission predominates. As shown in Figure 2d, the trion binding and emission energies are ≈30 meV and ≈1.63 eV (for monolayer $MoSe_2$) and ≈27 meV and ≈1.61 eV (for heterojunction), respectively. Due to dielectric screening effect, both the emission peaks of exciton and trion at the junction region show redshift compared to the bare $MoSe_2$.[28–30]

When an electron-hole pair locates in the same valley (either **K** or −**K** valley) with opposite spins, the exciton is a bright neutral exciton. The valley optical selection rule for interband transition correlates the excitonic valley pseudospin and the polarization of the photon: **K** (−**K**) valley bright exciton can be interconverted with a σ^+ (σ^-) circularly polarized photon. In monolayer $MoSe_2$, negatively (positively) charged trion is composed of exciton in the same valley and an additional electron (hole) in the opposite valley. Spin-valley locking and optical selection rules lead to emission helicity being tied to the spin of the electron in the trion.[31,32] This allows optical generation and addressability of valley

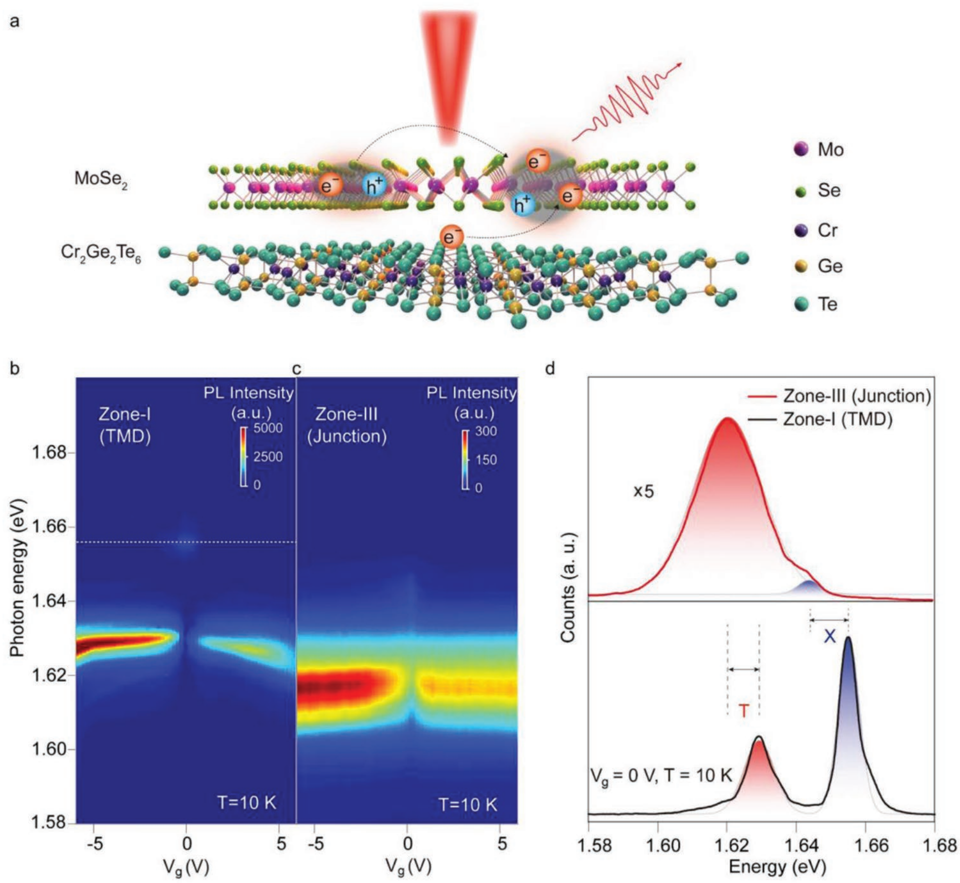

Figure 2. PL spectra of monolayer $MoSe_2$ and $Cr_2Ge_2Te_6$/$MoSe_2$ heterojunction. a) Schematics of crystal structure of $Cr_2Ge_2Te_6$/$MoSe_2$ heterojunction. PL spectra as a function of gate voltage in b) bare monolayer $MoSe_2$ and c) $Cr_2Ge_2Te_6$/$MoSe_2$ heterojunction. The white dash line represents the neutral exciton emission at the charge neutrality point. d) PL spectra of monolayer $MoSe_2$ and heterojunction at Vg = 0 V and 10 K. The PL spectra in the heterojunction can be well fitted by two Gaussian peaks, which are associated with trions and neutral excitons, respectively.

polarized excitons, along with trions. The degree of circular polarization (DOCP) can be depicted by[5]

$$\mathrm{DOCP} = \frac{I(\sigma^+) - I(\sigma^-)}{I(\sigma^+) + I(\sigma^-)} \tag{1}$$

where $I(\sigma^+)$ and $I(\sigma^-)$ are the left and right-handed circularly polarized PL intensities, respectively. The DOCP value characterizes the degree of valley polarization in the two valleys **K** (−**K**) of the monolayer $MoSe_2$.[33] To elucidate the exciton and trion magneto-optical response, we perform polarization resolved magneto-PL spectra in monolayer $MoSe_2$ and heterojunction. A schematic of the experimental setup is shown in Figure S6 (Supporting Information). The DOCP values of both exciton and trion in bare $MoSe_2$ under the polarized light of 1.75 eV are extremely low (≈0) and insensitive to the gate voltage (Figure S7, Supporting Information), which is consistent with previous results.[32,34]

We then investigate the gate-dependent magneto-DOCP map of the heterojunction, as plotted in **Figure 3**a. Two remarkable trends were immediately visible. First, the magnitude of DOCP is clearly larger as the gate voltage is ramped up to 80 V, as reflected by the increasingly dark colors toward the right of Figure 2a. Second, the polarity of the DOCP is seen to be inverted with the change of orientation of the external magnetic field. This is illustrated by the vertical change of colors, i.e., from blue to red, especially at higher gate voltages. The second observation is further magnified in Figure 3b, which displays two representative curves of the measured DOCP versus magnetic field at gate voltages (V_g) = 0 V and 80 V. Remarkably, the DOCP value at a positive 80 V gate is not only enlarged but also exhibits hysteresis behavior similar to the magnetic semiconductor $Cr_2Ge_2Te_6$ (See Figure 1d). The DOCP values at different gate voltages of the heterojunction could be obtained from Figure S8 (Supporting Information). To further illustrate the impact of gate voltage on DOCP values, we display the DOCP values as a function of gate voltage at 50 and −50 mT in Figure 3c. When we tune V_g from 0 to 80 V in the electron side, the DOCP values increase from ≈0 to ≈1.5%. Although the absolute value is not large, it is clearly identifiable within our experimental error. To clarify the interaction between the enhanced DOCP and the proximity effect of $Cr_2Ge_2Te_6$ and $MoSe_2$, temperature-dependent saturation magnetization (M_S) of $Cr_2Ge_2Te_6$ and DOCP values are plotted in Figure 3d. A significant drop of M_S of $Cr_2Ge_2Te_6$ is observed at 50 K, in agreement of T_C obtained in such typical few-layer $Cr_2Ge_2Te_6$.[23] Error bars in Figure 3(c),(d) indicate the standard deviation of DOCP or Ms at magnetization saturation. It is interesting to note that the DOCP difference also vanished at ≈50 K. We then attribute the strengthened DOCP in the heterojunction to the proximity effect of interface between $Cr_2Ge_2Te_6$ and $MoSe_2$.

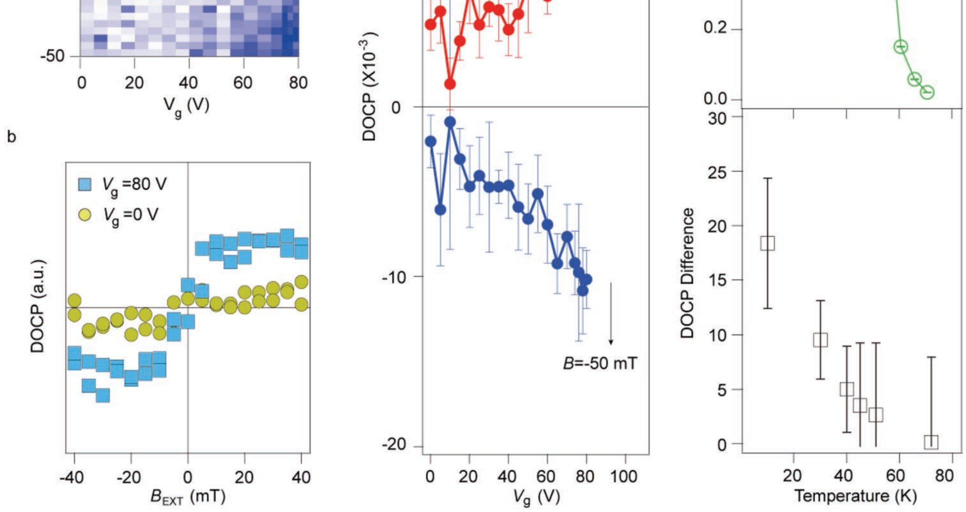

Figure 3. Electrically and magnetically tunable valley polarization in $Cr_2Ge_2Te_6/MoSe_2$ heterojunctions. a) Color map of DOCP for trions in the heterojunction as a function of gate voltage and applied magnetic field. b) DOCP as a function of magnetic field at $V_g = 0$ V and $V_g = 80$ V. c) Gate-dependent DOCP at ± 50 mT. d) Temperature-dependent saturation magnetization (M_S) of $Cr_2Ge_2Te_6$ and DOCP values of the heterojunction.

2.2. Band Alignment and Zeeman Splitting at $Cr_2Ge_2Te_6/MoSe_2$ Heterostructure

To reveal the physical origin of the observed polarization dynamics and the roles the heterojunction plays, we have carried out further investigations and analysis. First, it can be seen from Figure 2c that the line width of trions at the region of heterojunction is broadened compared with bare $MoSe_2$. There can be many reasons that lead to line width broadening, including impurities at the interface, enhanced thermal phonon scattering, and charge transfer.[35,36] But in the case of $Cr_2Ge_2Te_6/MoSe_2$ heterojunction, the dominant factor for the broadening may be charge transfer. Figure S9 (Supporting Information) presents the spatial correlation of the PL intensity of monolayer $MoSe_2$ and heterojunction. It can be noted that when the emission of trions becomes more pronounced in the heterojunction, the emission of neutral excitons decreases correspondingly, which is a signature of charge transfer. In addition, the intensities of excitonic states emission from the heterojunction is about one order of magnitude smaller than the bare $MoSe_2$. The quenching of emission in the $Cr_2Ge_2Te_6/MoSe_2$ heterojunction also supports efficient charge transfer at the interface.[17,35] We have carried out power-dependent PL spectra for the bare monolayer $MoSe_2$ and heterojunction, as shown in Figure S10 (Supporting Information). The power law $I \propto P^{\alpha}$ is used to fit the experimental data, where I, P, and α are the PL peak intensity, excitation power, and exponent factor, respectively. From the fitting results, the obtained α values of neutral exciton and trion emission in monolayer $MoSe_2$ are 0.96 and 1.01, respectively, presenting a linear dependence on the excitation power. However, the obtained α values of neutral exciton and trion emission in the heterojunction are 0.72 and 1.07, respectively. The sublinear power-dependent emission of neutral exciton in the heterojunction may originate from the free-to-bound transitions.[37]

To further identify the origin of the observed DOCP in the heterojunction and determine the band alignment, we performed KPFM measurements for the $Cr_2Ge_2Te_6/MoSe_2$ heterojunction on conductive Si substrate. Since the work function of $Cr_2Ge_2Te_6$ is dependent on the number of layers, we chose $Cr_2Ge_2Te_6$ flakes with similar thicknesses among the samples measured by PL.[38] To prevent degeneration, the stack of the heterojunction is constructed in the glove box and then measured by AFM as soon as possible. As shown in Figure S11 (Supporting Information), the surface potential of monolayer $MoSe_2$ decreases by about 100–200 meV upon stacking by few layer $Cr_2Ge_2Te_6$. Therefore, the work function of monolayer $MoSe_2$ is higher than that of few layer $Cr_2Ge_2Te_6$. Considering the bandgap and affinity of $Cr_2Ge_2Te_6$ and $MoSe_2$,[38,39] they are likely to form type-II band alignment, as illustrated in **Figure 4**a. The rectifying behavior of the heterojunction in Figure S3 (Supporting Information) further confirms the built-in potential at the interface.

When the heterojunction is illuminated by the laser, electron-hole pairs are excited in the conduction bands (CB) and valance bands (VB) of monolayer $MoSe_2$ and $Cr_2Ge_2Te_6$, respectively. Because the energy of CBs for $MoSe_2$ and $Cr_2Ge_2Te_6$ are very close, the photogenerated electrons in $Cr_2Ge_2Te_6$ are transferred to the CB of $MoSe_2$. In the case of applying magnetic fields, the photogenerated electrons in $Cr_2Ge_2Te_6$ are spin aligned with $Cr_2Ge_2Te_6$ majority-spin states and will be able to efficiently transfer to CB of $MoSe_2$. However, due to the large valence band offset between $MoSe_2$ and $Cr_2Ge_2Te_6$, the photogenerated holes in $MoSe_2$ are prohibited to move to $Cr_2Ge_2Te_6$, even at large negative gate voltage. As a result, the electron-hole pairs in $MoSe_2$ and the spin-polarized electrons introduced from the neighboring $Cr_2Ge_2Te_6$ are more favorable for the formation of trions. Because of the optical selection rules and spin-valley locking in TMDs, the spin-polarized trions will give rise to an enhanced valley polarization as shown in Figure 3c. Moreover,

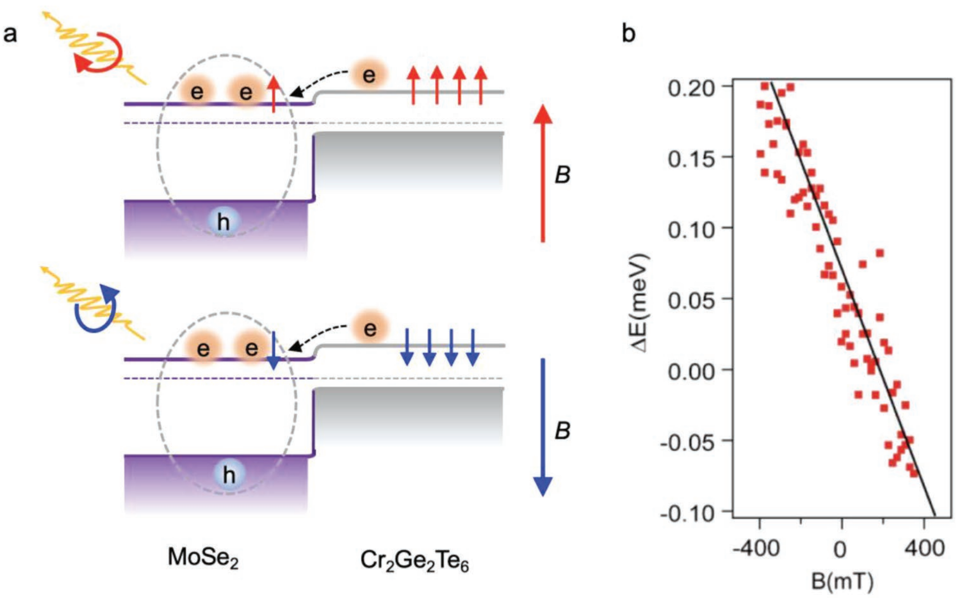

Figure 4. Band alignment and valley splitting of $Cr_2Ge_2Te_6/MoSe_2$ heterojunctions. a) Schematic illustration of spin-polarized charge transfer phenomena and trion formation in the $MoSe_2/Cr_2Ge_2Te_6$ heterojunction when a magnetic field is applied. b) Plots of Zeeman splitting energy versus magnetic field with linear fits for the trions.

when the applied gate voltage increases, the spin-polarized electrons in $Cr_2Ge_2Te_6$ can transfer to $MoSe_2$ more efficiently due to the enlarged vertical field, leading to the increased DOCP value of trions in the heterojunction as displayed in Figure 3c.

Moreover, valley splitting of trions can be observed in the heterojunction with out-of-plane magnetization, as shown in Figure 4b (Figure S12, Supporting Information). The obtained valley splitting rate is estimated to be ≈0.6 meV/T, which is several times larger than that can be achieved by the Zeeman effect in bare $MoSe_2$.[40,41] Note that the large valley splitting rate of the heterojunction is also observed in other TMD/FM systems,[17,42] indicating the presence of the proximity effects in the interface between $MoSe_2$ and $Cr_2Ge_2Te_6$. Another essential topic for further study is whether we could observe similar or better results of gate-tunable DOCP in other TMD-based vdW magnetic heterojunctions. For example, in stark contrast to $MoSe_2$, the degree of valley polarization in monolayer WSe_2 is much larger. However, DOCP in our fabricated $Cr_2Ge_2Te_6/WSe_2$ heterojunctions exhibited negligible gate tunability. This unexpected result indicates there may be other important factors that can influence the magnetic proximity effect of heterojunctions, such as interfacial exchange coupling and type-II band alignment.[16,17] We emphasize that further theoretical studies and detailed experiments will be required to fully understand the gate-tunable magnetic proximity effect in other $Cr_2Ge_2Te_6$-interfaced TMD systems.

In summary, we have investigated the gate-dependent circularly polarized photoluminescence in monolayer $MoSe_2$ interfaced with 2D ferromagnetic semiconductor $Cr_2Ge_2Te_6$. Significantly, the observed trion DOCP in the heterojunction exhibits magnetic hysteresis loop behavior that inherits from the neighboring magnetic semiconductor. The DOCP of the heterojunction is seen to be electrically manipulated or enhanced by a gate voltage that encourages electron hopping from the $Cr_2Ge_2Te_6$ side into the TMD monolayer. The DOCP's temperature dependence and enlarged Zeeman splitting points to interfacial magnetic exchange field as the underlying physical mechanism. Our findings shed new light on the mechanisms of interlayer charge transfer in 2D TMD/ferromagnetic semiconductor van der Waals interfaces and represent an important step forward in devising field-controlled 2D magneto-optoelectronic devices.

3. Experimental Section

Device Fabrication: Monolayer $MoSe_2$, h-BN, and few-layer graphene flakes were mechanically exfoliated from bulk crystal onto silicon substrates with a 300 nm SiO_2. Monolayers of $MoSe_2$ were identified by optical contrast and PL measurements, while the thickness of h-BN flakes was determined with atomic force microscopy. First, h-BN (≈20–30 nm) was used to pick up the monolayer $MoSe_2$ by dry transfer technique and flipped the stacks on PPC on bare substrates. Then the stacks were annealed in a high vacuum furnace at 300 °C for 1 h to ensure the cleanness of the monolayer $MoSe_2$ and bottom h-BN. Due to the instability of $Cr_2Ge_2Te_6$, few-layered $Cr_2Ge_2Te_6$ flakes were exfoliated onto PDMS and identified their thickness by optical contrast in a glove box with O_2 and H_2O levels below 0.1 parts per million. After the proper $Cr_2Ge_2Te_6$ samples were found, the $Cr_2Ge_2Te_6$ samples were transferred onto the pre-prepared $MoSe_2$/h-BN heterostructure. In order to complete the encapsulation of $MoSe_2/Cr_2Ge_2Te_6$ heterojunction between h-BN layers, another h-BN (20–30 nm) with two graphite flakes was further picked up and transferred onto the $Cr_2Ge_2Te_6/MoSe_2$/h-BN heterostructure to form h-BN/graphite/$Cr_2Ge_2Te_6/MoSe_2$/h-BN. The two pieces of graphite flakes were used as electrodes to contact $Cr_2Ge_2Te_6$. Next, electrical contacts to graphite flakes and $MoSe_2$ were defined with electron-beam lithography and deposited via thermal evaporation (5 nm chromium and 50 nm gold).

Magneto-Optic Kerr Effect (MOKE) Measurements: The experiments were performed in a closed-cycle optical cryostat at a sample temperature of 10 K unless special notification. The samples can be positioned to scan by a nano-precision *x-y-z* piezo stage. A linear polarized laser of 1.73 eV was focused on the sample surface in Faraday geometry with respect to the magnetic field up to 400 mT. The focused spot diameter was estimated to 2 µm. The reflected laser was analyzed by a half-wave plate and a Wollaston prism and collected by a balanced photoreceiver. More technical details can be referred in ref. [21].

Photoluminescence Measurements: To measure photoluminescence (PL) of the samples, a mode-locked Ti: Sapphire laser with a photon energy of 1.75 eV was used for sample excitation. The spatial resolution of PL was similar to MOKE. After filtered by a long-pass filter, the PL photons were coupled to a Horiba iHR550 monochromator with a liquid nitrogen cooled CCD detector (Horiba, Symphony II). For DOCP measurements, the polarization of excitation laser was controlled by a calibrated liquid crystal retarder. The helicity of PL was distinguished by a quarter retardance and a Glan–Thompson prism. All the optics in the measurements were achromatic in the studied spectrum range to minimize the chromatic aberration.

Supporting Information

Supporting Information is available from the Wiley Online Library or from the author.

Acknowledgements

This work was supported by the National Key R&D Program of China (Nos. 2017YFA0206304, 2018YFB2200500, and 2019YFA0307800), and supported by the National Natural Science Foundation of China (NSFC) (Grant Nos. 12004259, 12104462, 11974357, and U1932151), and China Postdoctoral Science Foundation (Grant No. 2019M663046). H.L. was supported by Ministry of Science and Technology of China (Grant No. 2018YFE0202600), Beijing Natural Science Foundation (Grant No. Z200005).

Conflict of Interest

The authors declare no conflict of interest.

Author Contributions

T.Z., S.Z., A.W. contributed equally to this work. F.W., Z.H., and S.Z. supervised the overall project. S.Z. fabricated and characterized the samples. T. Z., A.W., and F.W. conducted the MOKE and PL measurements. Z.X. contributed to the DOCP measurements. Y.L. contributed to KPFM measurements. M.X. and H.L. synthesized the bulk material of $Cr_2Ge_2Te_6$. S.Z., T.Z., and F.W. analyzed and interpreted all data, and S.Z. wrote the manuscript with discussions from all authors.

Data Availability Statement

The data that support the findings of this study are available from the corresponding author upon reasonable request.

Keywords

heterostructures, transition metal dichalcogenides, two-dimensional ferromagnetic semiconductors, valley polarization

Received: April 27, 2022
Revised: May 24, 2022
Published online: June 11, 2022

[1] K. F. Mak, D. Xiao, J. Shan, *Nat. Photonics* **2018**, *12*, 451.
[2] G. Wang, A. Chernikov, M. M. Glazov, T. F. Heinz, X. Marie, T. Amand, B. Urbaszek, *Rev. Mod. Phys.* **2018**, *90*, 021001.
[3] S. Zhao, X. Li, B. Dong, H. Wang, H. Wang, Y. Zhang, Z. Han, H. Zhang, *Rep. Prog. Phys.* **2021**, *84*, 026401.
[4] K. L. Seyler, P. Rivera, H. Yu, N. P. Wilson, E. L. Ray, D. G. Mandrus, J. Yan, W. Yao, X. Xu, *Nature* **2019**, *567*, 66.
[5] K. F. Mak, K. He, J. Shan, T. F. Heinz, *Nat. Nanotechnol.* **2012**, *7*, 494.
[6] H. Zeng, J. Dai, W. Yao, D. Xiao, X. Cui, *Nat. Nanotechnol.* **2012**, *7*, 490.
[7] T. Cao, G. Wang, W. Han, H. Ye, C. Zhu, J. Shi, Q. Niu, P. Tan, E. Wang, B. Liu, J. Feng, *Nat. Commun.* **2012**, *3*, 887.
[8] S. Cha, M. Noh, J. Kim, J. Son, H. Bae, D. Lee, H. Kim, J. Lee, H. Shin, S. Sim, S. Yang, S. Lee, W. Shim, C. Lee, M. Jo, J. S. Kim, D. Kim, H. Choi, *Nat. Nanotechnol.* **2018**, *13*, 910.
[9] L. Li, L. Shao, X. Liu, A. Gao, H. Wang, B. Zheng, G. Hou, K. Shehzad, L. Yu, F. Miao, Y. Shi, Y. Xu, X. Wang, *Nat. Nanotechnol.* **2020**, *15*, 743.
[10] X. Wang, J. Zhu, K. L. Seyler, P. Rivera, H. Zheng, Y. Wang, M. He, T. Taniguchi, K. Watanabe, J. Yan, D. G. Mandrus, D. R. Gamelin, W. Yao, X. Xu, *Nat. Nanotechnol.* **2021**, *16*, 1208.
[11] T. Norden, C. Zhao, P. Zhang, R. Sabirianov, A. Petrou, H. Zeng, *Nat. Commun.* **2019**, *10*, 4163.
[12] Y. Wan, J. Xiao, J. Li, X. Fang, K. Zhang, L. Fu, P. Li, Z. Song, H. Zhang, Y. Wang, M. Zhao, J. Lu, N. Tang, G. Ran, X. Zhang, Y. Ye, L. Dai, *Adv. Mater.* **2018**, *30*, 1703888.
[13] Z. Li, C. Liu, X. Rong, Y. Luo, H. Cheng, L. Zheng, F. Lin, B. Shen, Y. Gong, S. Zhang, Z. Fang, *Adv. Mater.* **2018**, *30*, 1801908.
[14] A. Ciarrocchi, D. Unuchek, A. Avsar, K. Watanabe, T. Taniguchi, A. Kis, *Nat. Photonics* **2019**, *13*, 131.
[15] D. Unuchek, A. Ciarrocchi, A. Avsar, Z. Sun, K. Watanabe, T. Taniguchi, A. Kis, *Nat. Nanotechnol.* **2019**, *14*, 1104.
[16] T. P. Lyons, D. Gillard, A. Molina-Sánchez, A. Misra, F. Withers, P. S. Keatley, A. Kozikov, T. Taniguchi, K. Watanabe, K. S. Novoselov, J. Fernández-Rossier, A. I. Tartakovskii, *Nat. Commun.* **2020**, *11*, 6021.
[17] D. Zhong, K. Seyler, X. Lingpeng, R. Cheng, N. Sivadas, B. Huang, W. Schmidgall, T. Taniguchi, K. Watanabe, M. A. McGuire, W. Yao, D. Xiao, K. C. Fu, X. Xu, *Sci. Adv.* **2017**, *3*, e1603113.
[18] K. L. Seyler, D. Zhong, B. Huang, X. Linpeng, N. P. Wilson, T. Taniguchi, K. Watanabe, W. Yao, D. Xiao, M. A. McGuire, K. C. Fu, X. Xu, *Nano Lett.* **2018**, *18*, 3823.
[19] Z. Wang, I. Gutiérrez-Lezama, N. Ubrig, M. Kroner, M. Gibertini, T. Taniguchi, K. Watanabe, A. Imamoğlu, E. Giannini, A. F. Morpurgo, *Nat. Commun.* **2018**, *9*, 2516.
[20] Z. Wang, I. Gutiérrez-Lezama, D. Dumcenco, N. Ubrig, T. Taniguchi, K. Watanabe, E. Giannini, M. Gibertini, A. F. Morpurgo, *Nat. Commun.* **2021**, *12*, 6659.
[21] Z. Wang, T. Zhang, M. Ding, B. Dong, Y. Li, M. Chen, X. Li, J. Huang, H. Wang, X. Zhao, Y. Li, D. Li, C. Jia, L. Sun, H. Guo, Y. Ye, D. Sun, Y. Chen, T. Yang, J. Zhang, S. Ono, Z. Han, Z. Zhang, *Nat. Nanotechnol.* **2018**, *13*, 554.
[22] I. A. Verzhbitskiy, H. Kurebayashi, H. Cheng, J. Zhou, S. Khan, Y. P. Feng, G. Eda, *Nat. Electron.* **2020**, *3*, 460.
[23] C. Gong, L. Li, Z. Li, H. Ji, A. Stern, Y. Xia, T. Cao, W. Bao, C. Wang, Y. Wang, Z. Q. Qiu, R. J. Cava, S. G. Louie, J. Xia, X. Zhang, *Nature* **2017**, *546*, 265.
[24] Y. Liu, C. Petrovic, *Phys. Rev. B* **2017**, *96*, 054406.
[25] K. Shayan, N. Liu, A. Cupo, Y. Ma, Y. Luo, V. Meunier, S. Strauf, *Nano Lett.* **2019**, *19*, 7301.
[26] L. Wang, I. Meric, P. Y. Huang, Q. Gao, Y. Gao, H. Tran, T. Taniguchi, K. Watanabe, L. M. Campos, D. A. Muller, J. Guo, P. Kim, J. Hone, K. L. Shepard, C. R. Dean, *Science* **2013**, *342*, 614.
[27] S. Jiang, L. Li, Z. Wang, J. Shan, K. F. Mak, *Nat. Electron.* **2019**, *2*, 159.
[28] S. Borghardt, J. Tu, F. Winkler, J. Schubert, W. Zander, K. Leosson, B. E. Kardynał, *Phys. Rev. Mater.* **2017**, *1*, 054001.
[29] A. Raja, A. Chaves, J. Yu, G. Arefe, H. M. Hill, A. F. Rigosi, T. C. Berkelbach, P. Nagler, C. Schüller, T. Korn, C. Nuckolls, J. Hone, L. E. Brus, T. F. Heinz, D. R. Reichman, A. Chernikov, *Nat. Commun.* **2017**, *8*, 15251.
[30] E. Lorchat, L. E. Parra López, C. Robert, D. Lagarde, G. Froehlicher, T. Taniguchi, K. Watanabe, X. Marie, S. Berciaud, *Nat. Nanotechnol.* **2020**, *15*, 283.
[31] H. Yu, X. Cui, X. Xu, W. Yao, *Natl. Sci. Rev.* **2015**, *2*, 57.
[32] Y. Zhang, K. Shinokita, K. Watanabe, T. Taniguchi, M. Goto, D. Kan, Y. Shimakawa, Y. Moritomo, T. Nishihara, Y. Miyauchi, K. Matsuda, *Adv. Mater.* **2020**, *32*, 2003501.
[33] J. Sung, Y. Zhou, G. Scuri, V. Zólyomi, T. I. Andersen, H. Yoo, D. S. Wild, A. Y. Joe, R. J. Gelly, H. Heo, S. J. Magorrian, D. Bérubé, A. M. Mier Valdivia, T. Taniguchi, K. Watanabe, M. D. Lukin, P. Kim, V. I. Fal'ko, H. Park, *Nat. Nanotechnol.* **2020**, *15*, 750.
[34] V. Kravtsov, T. Ivanova1, A. N. Abramov, P. V. Shilina, P. O. Kapralov, D. N. Krizhanovskii, V. N. Berzhansky, V. I. Belotelov, I. A. Shelykh, A. I. Chernov, I. V. Iorsh, *2D Mater.* **2022**, *9*, 015019.
[35] A. F. Rigosi, H. M. Hill, Y. Li, A. Chernikov, T. F. Heinz, *Nano Lett.* **2015**, *15*, 5033.
[36] J. Dang, M. Yang, X. Xie, Z. Yang, D. Dai, Z. Zuo, C. Wang, K. Jin, X. Xu, *Small* **2021**, *17*, 2106029.
[37] T. Schmidt, K. Lischka, W. Zulehner, *Phys. Rev. B* **1992**, *45*, 8989.
[38] S. Rahman, B. Liu, B. Wang, Y. Tang, Y. Lu, *ACS Appl. Mater. Interfaces* **2021**, *13*, 7423.
[39] M. Grzeszczyk, M. R. Molas, K. Nogajewski, M. Bartoš, A. Bogucki, C. Faugeras, P. Kossacki, A. Babiński, M. Potemski, *Sci. Rep.* **2020**, *10*, 4981.
[40] Y. Li, J. Ludwig, T. Low, A. Chernikov, X. Cui, G. Arefe, Y. D. Kim, A. M. van der Zande, A. Rigosi, H. M. Hill, S. H. Kim, J. Hone, Z. Li, D. Smirnov, T. F. Heinz, *Phys. Rev. Lett.* **2014**, *113*, 266804.
[41] D. MacNeill, C. Heikes, K. F. Mak, Z. Anderson, A. Kormányos, V. Zólyomi, J. Park, D. C. Ralph, *Phys. Rev. Lett.* **2015**, *114*, 037401.
[42] C. Zhao, T. Norden, P. Zhang, P. Zhao, Y. Cheng, F. Sun, J. P. Parry, P. Taheri, J. Wang, Y. Yang, T. Scrace, K. Kang, S. Yang, G. Miao, R. Sabirianov, G. Kioseoglou, W. Huang, A. Petrou, H. Zeng, *Nat. Nanotechnol.* **2017**, *12*, 757.

